Septins and a formin have distinct functions in chiral cortical rotation in the anaphase *C. elegans* zygote.

Adhham Zaatri, Jenna A. Perry, and Amy Shaub Maddox*

Department of Biology, UNC-Chapel Hill

*To whom correspondence should be addressed (asm@unc.edu)

Abstract

Many cells and tissues exhibit chirality that stems from the chirality of constituent proteins and polymers. For example, the *C. elegans* zygote undergoes an actomyosin-driven chiral rotation in which the entire cortex is displaced circumferentially around the division plane during anaphase. This phenomenon thus relates to how force and chirality are translated across scales. Although it is known that actomyosin contractility drives this rotation, its molecular mechanisms are incompletely understood. Septins are candidates for contributing to cell-scale chirality due to their ability to anchor and organize the actomyosin cytoskeleton. Here, we report that septins are required for anaphase cortical rotation. In contrast, the formin CYK-1, which we found to be enriched in the posterior in early anaphase, is not required for cortical rotation, but contributes to its chirality. Simultaneous loss of septin and CYK-1 function led to highly abnormal and often reversed cortical rotation. We propose a model by which anaphase cortical contractility is biased in a chiral fashion via interaction between the circumferential cytokinetic ring and perpendicular, longitudinal formin-based actin bundles that have accumulated torsional stress during formin-based polymerization. Our findings thus shed light on the molecular and physical bases for cellular

chirality in the *C. elegans* zygote. We also identify conditions in which chiral rotation fails but animals are developmentally viable, opening avenues for future work on the relationship between early embryonic cellular chirality and animal body plan.

Introduction

Chirality is an intrinsic feature of proteins, subcellular structures, cells, organs and organisms. Large scale chirality can emerge from fluid flows and contraction (reviewed in Pohl, 2015). Cellular chirality is attributed to the chirality of constituent proteins and other biomolecules, but how this asymmetry or handedness is translated several orders of magnitude in length scale from molecule to cell is poorly understood. The polymerization of cytoskeletal proteins into much larger filaments is an excellent candidate for the scaling-up of chirality information.

C. elegans undergoes deterministic development; blastomeres adopt specific fates as early as their birth during cleavages and body axes are established early (Sulston et al., 1983). Even in the one-cell embryo (zygote), where only the anterior-posterior axis is initially apparent, several rotational cortical flows with consistent chirality/handedness occur. In early anaphase, the entire cortex of the cell rotates, flowing about the anterior-posterior axis with a right-handed chirality, defined as flows resembling the curl of right hand fingers when the right hand thumb is pointed to the posterior (Figure 1a) (Naganathan et al., 2014; Schonegg et al., 2014). This cortical rotation depends on zygote anterior-posterior polarity and is implicated in the cortical chirality of early blastomeres and establishment of the dorso-ventral body axis, but is independent from the left-right axis of the body plan (Schonegg et al., 2014). While other asymmetrically-dividing blastomeres present in early development also exhibit this "net-rotating flow" in which the entire cortex rotates in the same direction, symmetrically-dividing blastomeres instead exhibit chiral counter-rotation, during which cortex in the posterior half flows around the circumference with

right-handed chirality, while cortex in the anterior half flows with left-handed chirality (Pimpale et al., 2020). In addition, cortex flows from the posterior to the anterior during embryo polarization (Hird & White, 1993). Concurrently with polarization, cortex in the anterior and posterior halves undergo counter-rotating flows, with, as in cytokinesis, the posterior half exhibiting right-handedness and the anterior half flowing with a left-handed chirality (Naganathan et al., 2014). Finally, during cytokinesis, the cortex flows into the cell equator, as observed throughout phylogeny (Khaliullin et al., 2018; White & Borisy, 1983). Cortical flows affect spindle positioning and therefore division plane specification and the placement and intercellular contacts of the resulting cells (Sugioka & Bowerman, 2018). Thus, defining the mechanisms controlling and executing flows may generate insights into developmental morphogenesis.

Cortical rotation in the anaphase *C. elegans* zygote depends on the actomyosin and microtubule cytoskeletons (Schonegg et al., 2014). Non-muscle myosin II drives contractility and remodeling of the actin cytoskeleton (Koenderink & Paluch, 2018). Both the activity levels and spatial patterning of both actin polymerization and non-muscle myosin II are controlled by the small GTPase RhoA, which itself is patterned by the microtubule cytoskeleton (Naganathan et al., 2014; Singh et al., 2019). Further mechanistic insight into cellular chirality is gained from work with adherent cultured mammalian cells in which initially radial actomyosin bundles are constructed and gradually adopt a chiral tilt, in a manner dependent on actomyosin contractility and actin polymerization by formins, which act in association with the membrane where they are activated by RhoA (Tee et al., 2015). This cell chirality also depends on crosslinking of radial and circumferential cytoskeletal bundles.

Septins are cytoskeletal proteins that form membrane-associated polymers that directly bind several components of the cortical cytoskeleton including F-actin and non-muscle myosin II. Septins have roles in cell division and cytoskeletal remodeling (Weirich et al., 2008) via their

contributions to the cortical localization of many cytoskeletal components and their regulators (Joo et al., 2007; Spiliotis & Gladfelter, 2012). In this capacity, septins contribute to cellular asymmetries (Gilden & Krummel, 2010; Maddox et al., 2007; Mostowy & Cossart, 2012) and to symmetry-breaking of actin-based structures (Maddox et al., 2007; Mavrakis et al., 2014; Spiliotis, 2010). That said, *C. elegans* septins are dispensable for zygote anterior-posterior polarity (Davies et al., 2016; Nguyen et al., 2000), and for zygote cytokinesis, though septin depletion does cause the zygote cytokinetic ring to close abnormally concentrically (Maddox et al., 2007). *C. elegans* septins form a non-polar heterotetramer composed of UNC-59 at the ends and UNC-61 in the middle (John et al., 2007; Nishihama et al., 2011). Septins are thus candidates for crosslinking actin-based structures and for scaffolding formin-generated F-actin at the membrane (Akhmetova et al., 2018; Breitsprecher & Goode, 2013; Buttery et al., 2012; Gao et al., 2010). Septins' roles in cortical rotation have been examined in highly compressed *C. elegans* zygotes that are sensitized to fail cytokinesis, and in which the integrity of longitudinal (anterior-posterior) myosin bundles is implicated in rotation (Singh et al., 2019). Septins are required for rotation in this condition, but their role in cellular chirality in less deformed cells was not known (Singh et al., 2019).

Here we compared wild-type *C. elegans* zygotes with those depleted of the septin UNC-59, and from strains with loss-of-function mutations in both genes that encode septins, *unc-59* and *unc-61*. Qualitative assessment of cortical rotation as well as quantification by particle image velocimetry (PIV) (Liberzon et al., 2019) demonstrated that septins are required for cortical rotation. To understand how septins transmitted polymer or molecular chirality to the cellular level, we interrogated the interplay between septins and the formin CYK-1. We observed an enrichment of GFP-tagged CYK-1 in the zygote posterior that was lost when septins were depleted. Loss of CYK-1 function also perturbed cortical rotation, but in a manner distinct from the effects resulting from septin loss of function. Simultaneous loss of function of the septin and CYK-1 largely

eliminated rotation, and caused randomization of rotation chirality. These findings begin to elucidate the roles of septins and CYK-1 in driving and controlling chiral rotation and suggest that septin scaffolding of the actomyosin cytoskeleton contributes to cellular chirality.

Methods

C. elegans strains and maintenance

C. elegans (see Table 1 for strain names and genotypes) were maintained on nematode growth medium (NGM) and OP50 bacterial food at 20ºC. Worms were transferred to new plates two days prior to imaging in non-RNAi experiments. The strain bearing CYK-1::GFP was previously published (Hirani et al., 2019).

The strain bearing *unc-59(e1005),* characterized and kindly provided by Julie Canman, bears G160-to-A160, not G85-to-A85 (encoding UNC-59 with Gly54-to-Arg54 not Gly29-to-Arg29) as previously described (Nguyen et al., 2000).

RNA-mediated protein depletion (RNAi)

Starved worms were grown on NGM-OP50 for 24 hours at 20ºC. 10-20 fourth larval stage (L4) worms were transferred onto an NGM plate containing 1mM IPTG and 0.132 mM carbenicillin, and seeded with bacteria expressing dsRNAs. Imaging began 20 hours from the start of RNAi feeding for CYK-1 depletion, or 24 hours for UNC-59 depletion.

Embryo mounting and image acquisition

Worms were mounted onto 2% agarose pad as previously described except that they were transferred from a drop on a cover glass and not via mouth pipet (Maddox & Maddox, 2012).

The same procedure was employed in mounting zygotes for measuring intensity of CYK-1::GFP except for the photobleaching control cells that were instead dissected in 1.5 µL of 0.1 M of Na++-Azide in M9 buffer.

For Figures 1-3, a DeltaVision Elite microscope (Cytiva) with an Olympus 60X 1.40 NA silicone oil immersion objective lens was used to image embryos by differential interference contrast. At a time interval of 2 seconds, two optical sections were acquired: the midplane of the cell (for timing anaphase onset) and the cortical plane (proximal to the coverslip). For Figure 3, CYK-1::GFP localization before rotation was imaged on the DeltaVision, and CYK-1::GFP timelapse image series were acquired on a Nikon A1R scanning confocal using a 60X 1.27 NA water immersion objective lens, and 3 second intervals.

To determine the handedness of cortical rotation imaged on our DeltaVision Elite microscope, we used the orientation of a printed letter "F" mounted on a microscope slide as a guide. In raw images, the letter F appeared mirrored, as compared to when viewed with the naked eye. To generate a true-to-life image orientation, therefore, we mirrored our images of *C. elegans* zygotes (in which cortical rotation had appeared to have left-handed chirality).

Image Analysis

The cortical plane of the movie was separated into a series of individual TIFF images using Fiji. The series of cortical images was then analyzed using OpenPIV, a Particle Image Velocimetry (PIV; http://www.openpiv.net/) plugin for Python (Liberzon, et al., 2019; Schindelin et al., 2012). Form the resulting vector field of the velocities, vectors perpendicular and parallel to the cell long axis were separately averaged.

Rotation intervals were determined by using a cutoff circumferential velocity of 0.09 micron/s, with the tolerance 0.01 micron/sec lower for the frame immediately before/after the

initially determined rotation period. Circumferential velocity is defined as speed in the right-handed direction perpendicular to the anterior-posterior axis. Anterior-posterior velocity is defined as speed directed towards the zygote posterior. Frames within the tolerance were discarded if less than four consecutive frames were accepted, with the heightened speed being attributed to stochastic movement or other processes.

Average velocity measurements used a range of +/- 2.5 microns from the manually defined central line of the cell. Positional velocity measurements average the velocity over the whole rotation interval by dividing the aforementioned region of interest into 20 bins along the anterior-posterior axis. The anterior-posterior axis was identified via the presence of polar bodies (anterior) and displacement of the anaphase spindle (posterior). Rotation type (as defined below; continuous, intermittent, alternating and none) was determined using the average velocity measurements. Continuous rotation had a single period of at least 38 seconds of circumferential velocity above 0.09 microns/sec. Intermittent rotation had at least one period above this velocity cutoff, separated by a period of velocity below the cutoff, but not negative, with little consistency in the duration of these periods; at least 8 seconds of heightened velocity was required for this classification. Alternating rotation had at least one period of rotation with circumferential velocity above 0.09 microns/sec followed by a period with a velocity of -0.09 microns/sec or below in the opposite direction for at least 8 seconds. No rotation meant that no frames met the previously described criteria for defining a period of rotation.

Fluorescence intensity was measured via Fiji for images acquired on the DeltaVision Elite. Background fluorescence intensity outside the cell was subtracted from all intensity measurements in the cell (see Figure 3A). For images recorded on the A1R, intensity was measured by specifying regions of interest pre-imaging and exported directly from the NIS-Elements imaging software. The change in intensity over time was fitted to an exponential decay curve.

Kymographs were made using Fiji's multi kymograph tool. A line of pixel width 10 was used. Lines were drawn perpendicular to the A-P axis; if the axis was oriented with Anterior on the left, the line was drawn from top to bottom. The interval was used ± 50 sec of the determined rotation interval for the cell.

Results

Quantifying cortical rotation

Cortical rotation in the *C. elegans* zygote is an example of cell-scale chirality whose mechanism may provide insights into how molecular chirality influences cell behavior. To uncover molecular mechanisms of this event, we first quantitatively analyzed zygote anaphase cortical rotation. We began by using DIC transmitted light microscopy to visualize zygotes during late metaphase and early anaphase. Cytoplasmic granules near the cortex of control *C. elegans* zygotes were displaced circumferentially around the cell, their trajectories exhibiting a right-handed chirality around the anterior-posterior axis (Figure 1A-C; Supplemental Movie 1), consistent with (Schonegg et al., 2014).

We used particle image velocimetry (PIV) to quantify cortical rotation by tracking the motion of particles between pairs of images, identifying patches of texture, such as cytoplasmic granules (Figure 1B), in the first image, then finding those same patches in the second image. PIV then generates a vector field of the speed of features in the images based on their displacement and the time between frames (Figure 1D). The vectors, representing the motion of cortical granules, moved around the cell circumference (around the anterior-posterior axis) with right-handed chirality.

The average speed for cortical rotation has been reported as 0.35 microns/second (Singh & Pohl, 2014). However, since particles are essentially stationary before anaphase cortical rotation, and rotation has a finite duration of 50-60 seconds (Schonegg et al., 2014), we sought to characterize the speed dynamics of rotation throughout its duration. We used the spatially- and temporally-resolved data from the vector field and found that cortical rotation first accelerated and then decelerated, peaking in the middle 10-12 seconds of rotation (Figure 1E). For any given timepoint during rotation, the vector field was notably uniform, with only slight variations in angle relative to the anterior-posterior axis. The average instantaneous velocity in the anterior-posterior direction was very low (Figure 1F). As previously described (Schonegg et al., 2014; Singh & Pohl, 2014), rotation velocity was relatively uniform along the length of the embryo (Figure 1G, H). Thus, the entire *C. elegans* zygote cortex undergoes a short-lived chiral rotation that displaces cortical material around the cell circumference.

Septins are required for cortical rotation

Cortical rotation in the *C. elegans* zygote is driven by contractility of the actomyosin cytoskeleton associated with the plasma membrane (Schonegg et al., 2014). Septins are implicated in linking these two cellular components; septins also contribute to cell cortex polarity in yeast (Bridges & Gladfelter, 2015) and furrowing asymmetry in the *C. elegans* zygote (Maddox et al., 2007). *C. elegans* septins are required for zygote anaphase chiral rotation in severely compressed cells, but are not required for the chiral counter-rotation during zygote polarization (Naganathan et al., 2018; Singh et al., 2019). Since cortical mechanics are affected by cell compression and therefore shape (Singh et al., 2019), we tested whether septins were required for zygote anaphase cortical rotation in cells that were not deformed beyond the slight compression arising from traditional mounting of *C. elegans* embryos (Pimpale et al., 2020).

We first depleted the septin UNC-59 via RNA-mediated interference (RNAi) and found that in many UNC-59 septin depleted cells, cortical rotation failed (Figure 2A, C, F & G, Figure 2 supplement, and Supplemental Movie 1). In UNC-59-depleted zygotes undergoing cortical rotation, both the maximal and average rotation velocity were reduced (Figure 2C, F, G). The duration of rotation was reduced in most cases (Figure 2H) and total distance was significantly reduced compared to controls (Figure 2I). Thus, as in severely compressed cells that fail cytokinesis (Singh et al., 2019), septins are required for normal cortical rotation in otherwise-healthy cells that complete cytokinesis (Maddox et al., 2007).

We next tested the effect of septin loss of function using *C. elegans* zygotes bearing a mutant allele of *unc-59*, encoding a point-mutated UNC-59 protein that fails to localize to the contractile ring in cytokinesis (*e1005*; Nguyen et al., 2000). When compared to UNC-59 depleted cells, zygotes from *unc-59(e1005)* were similar, often failing cortical rotation or rotating intermittently (Figure 2A, B, D and Supplemental Movie 1). As a population, a greater proportion of mutant cells failed rotation (Figure 2A), and individual mutant cells exhibited even lower maximal and average rotation velocities than UNC-59 depleted cells (Figure 2D, F & G).

Septin function is thought to be fully removed by depleting one septin or mutating one of the two genes; heterotetramerization of UNC-59 and UNC-61 is thought to stabilize each protein (John et al., 2007; Nishihama et al., 2011; Nguyen et al., 2000). Nevertheless, since differences in loss-of-function phenotypes exist (Hall et al., 2008) we wished to compare the loss-of-function allele of *unc-59* to a null allele of the other *C. elegans* septin gene *unc-61 (e228)*, which bears a premature stop codon and in which no UNC-61 protein is detected by blotting with an antibody recognizing the N-terminus (Nguyen et al., 2000). Zygotes from the *unc-61* mutant strain resembled UNC-59 depleted and *unc-59(e1005)* zygotes in all our measures: maximum and average velocity, duration, and distance (Figure 2). Specifically, they had lower maximum and

average speeds than control cells (Figure 2A, E - G). In sum, our findings demonstrated that three septin perturbations are essentially identical, and that septins are required for normal cortical rotation in *C. elegans* zygotes. Since the septins are not directly implicated in motor-driven force generation, these results suggest that an additional factor is involved in translating molecular- or polymer-scale chirality to the cellular level.

The formin CYK-1 is asymmetrically distributed in a septin-dependent manner

Two possible factors have been recently implicated in anaphase chiral rotation in the *C. elegans* zygote: anterior-posterior polarity and anterior-posterior myosin bundles (Pimpale et al., 2020; Singh et al., 2019). Thin film active fluid theory demonstrated that net chiral rotation (as occurs in the zygote in anaphase) is sensitive to lengthwise (anterior-posterior) cell polarity, such as the displacement of the division plane from the midplane of the cell, or anterior-posterior asymmetry of cortical contractility (Pimpale et al., 2020). The contribution of anterior-posterior polarity to cortical rotation is unlikely to explain rotation failure in septin loss-of-function cells, though, because septins are dispensable for zygote anterior-posterior polarity (Davies et al., 2016; Nguyen et al., 2000).

Another factor recently implicated in anaphase chiral rotation is the presence and integrity of "longitudinal" actomyosin bundles, extending between the anterior and posterior poles of the cell perpendicular to the cytokinetic ring (Singh et al., 2019). These bundles are assembled downstream of RhoA activity, but the source of F-actin within them was not examined. We hypothesized that the formin CYK-1, the only Dia family formin specific to cytokinesis in *C. elegans* (Davies et al., 2018), contributes to chiral cortical rotation. Since CYK-1 is dispensable for anterior-posterior polarity (Severson et al., 2002; Sönnichsen et al., 2005), perturbation of

CYK-1 allows interrogation of F-actin-based structures without perturbing division plane placement.

We began by examining the distribution of CYK-1 using cells expressing CYK-1 fluorescently tagged at its endogenous locus (CYK-1::GFP; Hirani et al., 2019). The invariant handedness of anaphase cortical rotation suggested that CYK-1 localization would be asymmetric, so we tested whether the distribution of CYK-1::GFP was polarized. CYK-1::GFP was slightly but consistently enriched in the zygote posterior immediately prior to anaphase onset (Figure 3A-C).

To begin to test whether loss of septin function could perturb cortical rotation by affecting CYK-1, we compared CYK-1::GFP polarization in control cells to those with incomplete septin function. Since the effects on cortical rotation of perturbing either septin were essentially indistinguishable (Figure 2), we depleted UNC-59 to test the effect of loss of septin function on CYK-1 localization. Following UNC-59 depletion, the posterior enrichment of CYK-1::GFP was eliminated (Figure 3B, C). From this, we concluded that the septins are required for the polarization of CYK-1.

Septins could impact polarized CYK-1 cortical enrichment indirectly, or more directly, by controlling its localization or stability. To begin to define CYK-1 cortical dynamics, we first performed time-lapse imaging of CYK-1::GFP and measured fluorescence intensity on the cortex, correcting for the calculated loss of fluorescence due to photobleaching (Figure 3 supplement). We found that leading up to anaphase onset and for the first minute of anaphase, when rotation occurs, levels of CYK-1::GFP on both the anterior and posterior poles of the cell increase over time (Figure 3 supplement). The relative enrichment of the formin on the posterior cortex also steadily rose (Figure 3D). By contrast, when the septin UNC-59 was depleted, CYK-1::GFP remained uniformly distributed (Figure 3D). In sum, these results demonstrate that the formin

CYK-1 is enriched in the posterior of the *C. elegans* zygote in a manner dependent on septins. This polarization suggested to us that CYK-1 also contributes to zygote chirality.

The formin CYK-1 and septins make distinct contributions to cortical rotation

The importance of anterior-posterior myosin bundles for chiral cortical rotation (Singh et al., 2019) and our observation of asymmetric CYK-1::GFP localization suggested that this formin contributes to chiral cortical rotation. This hypothesis was also supported by the observation that elimination of long F-actin bundles via inhibition of formins blocked chiral cytoskeletal morphologies in adherent mammalian cultured cells (Tee et al., 2015). To test whether the formin CYK-1 is important for chiral contractility in the *C. elegans* zygote, we used RNAi to slightly deplete CYK-1 such that all cells still completed cytokinesis, and quantified cortical rotation. Like septin loss-of-function, CYK-1 depletion reduced the proportion of zygotes exhibiting normal rotation (Figure 4 A-C, G, H, and Figure 4 supplement). Unlike septin perturbations, CYK-1 depletion did not reduce maximal or mean rotation speed (Figure 4E-F), but notably, in many CYK-1 depleted embryos, cortical rotation occurred with opposite handedness/chirality or alternating chirality (Figure 4A-C and Supplemental Movie 1). Furthermore, the duration of rotation and therefore total displacement were almost always (9/10) higher in CYK-1 depleted zygotes than in wild-type zygotes (Figure 4E-H). The wide range of abnormal cortical rotation effects following CYK-1 depletion likely reflects the incomplete and inconsistent cytoskeletal perturbations resulting from mild depletion of this essential protein. In sum, wild-type levels of the formin CYK-1 are dispensable for cortical rotation itself, but necessary for the consistent chirality of rotation.

Our results above suggested that septins and CYK-1 contribute to chiral cortical rotation in distinct ways: septins help translate contractility into whole-cell chiral movement, and the levels

and subcellular distribution of the formin CYK-1 contributes to the chirality of this contractility. Next, we sought to test the idea that they contribute in distinct ways by combining perturbations of the septin cytoskeleton and CYK-1. We depleted CYK-1 from *unc-61(e228)* zygotes and found that collectively, zygotes in which both CYK-1 and UNC-61 septin were perturbed exhibited more severe defects than those depleted of CYK-1 only; the average right-handed rotation velocity was essentially zero (Figure 4A, D, black line). This was because while some cells exhibited normal right-handed cortical rotation, others exhibited abnormal left-handed rotation. In general, rotation was slow, intermittent and often alternating between right- and left-handed rotation (Figure 4A, D). When directionality information was discarded, and speed was simply compared, zygotes in which both CYK-1 and UNC-61 septin were perturbed were statistically indistinguishable from *unc-61(e228)* zygotes (Figure 4E, F). These results support the hypothesis that septins and the formin CYK-1 contribute in distinct fashions to chiral cortical rotation: the formin directs the handedness of rotation while septins translate cytoskeletal chirality to whole-cell cortical rotation.

Discussion

Here, we show that the septins and a formin are required for chiral cortical rotation in anaphase in the *C. elegans* zygote. Specifically, rotation often fails when septins are depleted or mutated. We found that the F-actin nucleating- and elongating formin CYK-1, which we showed is slightly polarized to the zygote posterior, is also required for normal rotation. Unlike loss of septin function, CYK-1 depletion did not eliminate cortical flows but altered their chirality. Together, this work advances our understanding of how molecular-scale chirality is scaled up to the level of cell-scale behaviors. Formins related to CYK-1 have been implicated in the chirality of adherent mammalian cells (Tee et al., 2015), but gentler perturbations of formins will be necessary to discriminate between the requirement for formins for these cells' overall cytoskeletal

network architecture versus its chirality. Septins may play a role in cellular chirality in other species, but where many septin genes and combinatorial oligomers are present, achieving loss of septin function is difficult.

How does the cortex of the *C. elegans* zygote rotate inside of the eggshell? Our work connecting the septins and the formin CYK-1 to rotation, guided by published observations of cultured mammalian cells (Tee et al., 2015), suggests an explanation for this phenomenon (Figure 5). In mammalian cells, crosslinked perpendicular F-actin bundles accumulate the torsional stress of F-actin rotation as it is polymerized from membrane-anchored formins (Tee et al., 2015; Figure 5A). Accumulated stress is relieved by chiral displacement of initially-radial bundles. When the ventral-dorsal axis of adherent mammalian cells is equated to the anterior-posterior axis of the *C. elegans* zygote, we would predict that formins would be enriched in the posterior; we indeed observe a slight but consistent posterior enrichment (Figure 5Bi). We hypothesize that formins in the posterior produce F-actin bundles that emanate towards the cell anterior (Figure 5B and C, red). The cytokinetic ring then comprises perpendicular bundles (Figure 5B and C, gold) running circumferentially and intersecting with the posterior-to-anterior bundles. Accumulated chiral torsional stress in the latter bundles and mechanical coupling between the two populations of F-actin would bias contractility to drive movement with right-handed chirality.

How do septins translate non-muscle myosin II-driven contractility to cortical rotation? Septins are not directly implicated in the formation of F-actin filaments or bundles, but rather in several capacities that likely contribute to the accumulation of torsional stress associated with F-actin polymerization. First, as membrane-associated polymers, the septins could contribute to the anchoring of formins at the plasma membrane (Figure 5Bii and C, green 1). Without anchoring, the formin and the polymerizing F-actin could move freely relative to each other, and torsional stress would not accumulate. Furthermore, septins have been demonstrated to interact directly with

F-actin, anillin, and non-muscle myosin II (Spiliotis, 2010). Thus, septins may also contribute to cortical chirality by crosslinking within posterior-anterior bundles or within the cytokinetic ring, or between these two species of F-actin (Figure 5B and C, green 2-4). Uncoupling in any or all of these F-actin structures would be predicted to relieve polymerization-associated torsional stress and to reduce the lengthscale of the effect of local actomyosin contractility.

How does the formin CYK-1 contribute to the chirality of cortical flow and how does rotation occur with reversed (left-) handedness? The chirality of F-actin is invariant, as is the chirality of the torsional stress generated by formin-driven polymerization of actin into a highly crosslinked network. However, CYK-1 is only slightly enriched in the posterior, and mild depletion of CYK-1 may randomize or eliminate this asymmetry. Preferential or even intermittent interaction between circumferential cytokinetic ring F-actin and longitudinal bundles extending from the anterior towards the posterior would result in left-handed chirality of the anaphase contractile network (Figure 5Biii).

Chiral cortical rotation in the zygote represents the first appearance of handedness in a cell with radial symmetry around a single axis. Failure to establish body axes leads to early lethality (Belmont et al., 2004; Ware et al., 2004). Exploration of whether zygote chiral rotation is essential for viability has been limited because all other proteins reported to be required for this chirality are central to basic cell biological processes (*e.g.* tubulin, centrosome maturation machinery, the RhoGEF ECT-2, and non-muscle myosin II heavy chain; Schonegg et al., 2014). Although strains bearing septin loss-of-function alleles are viable, they exhibit a broad range of phenotypes including arrested development, uncoordinated movement, and vulval protrusion indicating tissue morphogenesis defects (Nguyen et al., 2000). It will be interesting to test, as we have in the past (Maddox et al., 2005), whether septin loss-of-function embryos with more severe cortical rotation phenotypes have decreased viability, or even randomized or reversed animal handedness, which is

tolerated in *C. elegans*, as it is in humans (Goldstein & Hird, 1996; Kosaki & Casey, 1998; Wood, 1991).

Acknowledgements

The authors are grateful to Julie Canman and her lab for characterizing and providing septin mutant strains. We thank Vincent Boudreau for creating tools in ImageJ, Iris Brammer for assistance in data collection, and Dylan Ray for technical assistance. For valuable discussion, we thank Bill Wood, Stephan Grill and Teije Middelkoop, and all the members of the Maddox labs. We thank Richard Cheney, Bob Goldstein, Michael Werner, and Ben Woods for critical reading of this manuscript.

References

Akhmetova, K. A., Chesnokov, I. N., & Fedorova, S. A. (2018). Functional Characterization of Septin Complexes. In *Molekuliarnaia biologiia*. https://doi.org/10.7868/S0026898418020015

Belmont, J. W., Mohapatra, B., Towbin, J. A., & Ware, S. M. (2004). Molecular genetics of heterotaxy syndromes. In *Current Opinion in Cardiology*. https://doi.org/10.1097/00001573-200405000-00005

Breitsprecher, D., & Goode, B. L. (2013). Formins at a glance. In *Journal of Cell Science*. https://doi.org/10.1242/jcs.107250

Bridges, A. A., & Gladfelter, A. S. (2015). Septin form and function at the cell cortex. *Journal of Biological Chemistry*. https://doi.org/10.1074/jbc.R114.634444

Buttery, S. M., Kono, K., Stokasimov, E., & Pellman, D. (2012). Regulation of the formin Bnr1 by septins and a MARK/Par1-family septin-associated kinase. *Molecular Biology of the Cell*. https://doi.org/10.1091/mbc.E12-05-0395

Davies, T., Jordan, S. N., & Canman, J. C. (2016). Cell polarity is on PAR with cytokinesis. In *Cell Cycle*. https://doi.org/10.1080/15384101.2016.1160667

Davies, T., Kim, H. X., Spica, N. R., Lesea-Pringle, B. J., Dumont, J., Shirasu-Hiza, M., & Canman, J. C. (2018). Cell-intrinsic and -extrinsic mechanisms promote cell-type-specific cytokinetic diversity. *ELife*. https://doi.org/10.7554/eLife.36204

Gao, L., Liu, W., & Bretscher, A. (2010). The yeast formin bnr1p has two localization regions that

show spatially and temporally distinct association with septin structures. *Molecular Biology of the Cell*. https://doi.org/10.1091/mbc.E09-10-0861

Gilden, J., & Krummel, M. F. (2010). Control of cortical rigidity by the cytoskeleton: Emerging roles for septins. In *Cytoskeleton*. https://doi.org/10.1002/cm.20461

Goldstein, B., & Hird, S. N. (1996). Specification of the anteroposterior axis in Caenorhabditis elegans. *Development*.

Hall, P. A., Maddox, A. S., Russell, S. E. H., & Pringle, J. R. (2008). The Septins. In *The Septins*. https://doi.org/10.1002/9780470779705

Hirani, N., Illukkumbura, R., Bland, T., Mathonnet, G., Suhner, D., Reymann, A. C., & Goehring, N. W. (2019). Anterior-enriched filopodia create the appearance of asymmetric membrane microdomains in polarizing C. elegans zygotes. *Journal of Cell Science*. https://doi.org/10.1242/jcs.230714

Hird, S. N., & White, J. G. (1993). Cortical and cytoplasmic flow polarity in early embryonic cells of Caenorhabditis elegans. *Journal of Cell Biology*. https://doi.org/10.1083/jcb.121.6.1343

John, C. M., Hite, R. K., Weirich, C. S., Fitzgerald, D. J., Jawhari, H., Faty, M., Schläpfer, D., Kroschewski, R., Winkler, F. K., Walz, T., Barral, Y., & Steinmetz, M. O. (2007). The Caenorhabditis elegans septin complex is nonpolar. *EMBO Journal*. https://doi.org/10.1038/sj.emboj.7601775

Joo, E., Surka, M. C., & Trimble, W. S. (2007). Mammalian SEPT2 Is Required for Scaffolding Nonmuscle Myosin II and Its Kinases. *Developmental Cell*. https://doi.org/10.1016/j.devcel.2007.09.001

Khaliullin, R. N., Green, R. A., Shi, L. Z., Gomez-Cavazos, J. S., Berns, M. W., Desai, A., & Oegema, K. (2018). A positive-feedback-based mechanism for constriction rate acceleration during cytokinesis in Caenorhabditis elegans. *ELife*. https://doi.org/10.7554/eLife.36073

Koenderink, G. H., & Paluch, E. K. (2018). Architecture shapes contractility in actomyosin networks. In *Current Opinion in Cell Biology*. https://doi.org/10.1016/j.ceb.2018.01.015

Kosaki, K., & Casey, B. (1998). Genetics of human left-right axis malformations. *Seminars in Cell and Developmental Biology*. https://doi.org/10.1006/scdb.1997.0187

Liberzon, Alex; Lasagna, Davide; Aubert, Mathias; Bachant, Pete; jakirkham; ranleu; tomerast; Käufer, Theo; Borg, Joe; Dallas, Cameron; Vodenicharski, B. (2019). *OpenPIV/openpiv-python*. https://zenodo.org/record/3566451

Maddox, Amy S., & Maddox, P. S. (2012). High-Resolution Imaging of Cellular Processes in Caenorhabditis elegans. In *Methods in Cell Biology*. https://doi.org/10.1016/B978-0-12-394620-1.00001-1

Maddox, Amy Shaub, Habermann, B., Desai, A., & Oegema, K. (2005). Distinct roles for two C. elegans anillins in the gonad and early embryo. *Development*. https://doi.org/10.1242/dev.01828

Maddox, Amy Shaub, Lewellyn, L., Desai, A., & Oegema, K. (2007). Anillin and the Septins Promote Asymmetric Ingression of the Cytokinetic Furrow. *Developmental Cell*. https://doi.org/10.1016/j.devcel.2007.02.018

Mavrakis, M., Azou-Gros, Y., Tsai, F. C., Alvarado, J., Bertin, A., Iv, F., Kress, A., Brasselet, S., Koenderink, G. H., & Lecuit, T. (2014). Septins promote F-actin ring formation by crosslinking actin filaments into curved bundles. *Nature Cell Biology*. https://doi.org/10.1038/ncb2921

Mostowy, S., & Cossart, P. (2012). Septins: The fourth component of the cytoskeleton. In *Nature Reviews Molecular Cell Biology*. https://doi.org/10.1038/nrm3284

Naganathan, S. R. a., Fürthauer, S., Nishikawa, M., Jülicher, F., & Grill, S. W. (2014). Active torque generation by the actomyosin cell cortex drives left-right symmetry breaking. *ELife*.

https://doi.org/10.7554/eLife.04165

Naganathan, S. R., Fürthauer, S., Rodriguez, J., Fievet, B. T., Jülicher, F., Ahringer, J., Cannistraci, C. V., & Grill, S. W. (2018). Morphogenetic degeneracies in the actomyosin cortex. *ELife*. https://doi.org/10.7554/eLife.37677

Nguyen, T. Q., Sawa, H., Okano, H., & White, J. G. (2000). The C. elegans septin genes, unc-59 and unc-61, are required for normal postembryonic cytokineses and morphogenesis but have no essential function in embryogenesis. *Journal of Cell Science*.

Nishihama, R., Onishi, M., & Pringle, J. R. (2011). New insights into the phylogenetic distribution and evolutionary origins of the septins. *Biological Chemistry*. https://doi.org/10.1515/BC.2011.086

Pimpale, L., Middelkoop, T. C., Mietke, A., & Grill, S. W. (2019). Cell lineage-dependent chiral actomyosin flows drive cellular rearrangements in early development. *BioRxiv*. https://doi.org/10.1101/842922

Pimpale, L., Middelkoop, T., Mietke, A., & Grill, S. (2020). Cell lineage-dependent chiral actomyosin flows drive cellular rearrangements in early C. elegans development. *ELife*. https://doi.org/10.7554/eLife.54930

Pohl, C. (2015). Cytoskeletal symmetry breaking and chirality: From reconstituted systems to animal development. In *Symmetry*. https://doi.org/10.3390/sym7042062

Schindelin, J., Arganda-Carreras, I., Frise, E., Kaynig, V., Longair, M., Pietzsch, T., Preibisch, S., Rueden, C., Saalfeld, S., Schmid, B., Tinevez, J. Y., White, D. J., Hartenstein, V., Eliceiri, K., Tomancak, P., & Cardona, A. (2012). Fiji: An open-source platform for biological-image analysis. In *Nature Methods*. https://doi.org/10.1038/nmeth.2019

Schonegg, S., Hyman, A. A., & Wood, W. B. (2014). Timing and mechanism of the initial cue establishing handed left-right asymmetry in Caenorhabditis elegans embryos. *Genesis*. https://doi.org/10.1002/dvg.22749

Severson, A. F., Baillie, D. L., & Bowerman, B. (2002). A Formin Homology protein and a profilin are required for cytokinesis and Arp2/3-independent assembly of cortical microfilaments in C. elegans. *Current Biology*. https://doi.org/10.1016/S0960-9822(02)01355-6

Singh, D., Odedra, D., Dutta, P., & Pohl, C. (2019). Mechanical stress induces a scalable switch in cortical flow polarization during cytokinesis. *Journal of Cell Science*. https://doi.org/10.1242/jcs.231357

Singh, D., & Pohl, C. (2014). Coupling of Rotational Cortical Flow, Asymmetric Midbody Positioning, and Spindle Rotation Mediates Dorsoventral Axis Formation in C. elegans. *Developmental Cell*. https://doi.org/10.1016/j.devcel.2014.01.002

Sönnichsen, B., Koski, L. B., Walsh, A., Marschall, P., Neumann, B., Brehm, M., Alleaume, A. M., Artelt, J., Bettencourt, P., Cassin, E., Hewitson, M., Holz, C., Khan, M., Lazik, S., Martin, C., Nitzsche, B., Ruer, M., Stamford, J., Winzi, M., … Echeverri, C. J. (2005). Full-genome RNAi profiling of early embryogenesis in Caenorhabditis elegans. *Nature*. https://doi.org/10.1038/nature03353

Spiliotis, E. T. (2010). Regulation of microtubule organization and functions by septin GTPases. In *Cytoskeleton*. https://doi.org/10.1002/cm.20448

Spiliotis, E. T., & Gladfelter, A. S. (2012). Spatial Guidance of Cell Asymmetry: Septin GTPases Show the Way. In *Traffic*. https://doi.org/10.1111/j.1600-0854.2011.01268.x

Sugioka, K., & Bowerman, B. (2018). Combinatorial Contact Cues Specify Cell Division Orientation by Directing Cortical Myosin Flows. *Developmental Cell*. https://doi.org/10.1016/j.devcel.2018.06.020

Sulston, J. E., Schierenberg, E., White, J. G., & Thomson, J. N. (1983). The embryonic cell lineage of the nematode Caenorhabditis elegans. In *Developmental Biology*.

https://doi.org/10.1016/0012-1606(83)90201-4

Tee, Y. H., Shemesh, T., Thiagarajan, V., Hariadi, R. F., Anderson, K. L., Page, C., Volkmann, N., Hanein, D., Sivaramakrishnan, S., Kozlov, M. M., & Bershadsky, A. D. (2015). Cellular chirality arising from the self-organization of the actin cytoskeleton. *Nature Cell Biology*. https://doi.org/10.1038/ncb3137

Ware, S. M., Peng, J., Zhu, L., Fernbach, S., Colicos, S., Casey, B., Towbin, J., & Belmont, J. W. (2004). Identification and Functional Analysis of ZIC3 Mutations in Heterotaxy and Related Congenital Heart Defects. *American Journal of Human Genetics*. https://doi.org/10.1086/380998

Weirich, C. S., Erzberger, J. P., & Barral, Y. (2008). The septin family of GTPases: Architecture and dynamics. In *Nature Reviews Molecular Cell Biology*. https://doi.org/10.1038/nrm2407

White, J. G., & Borisy, G. G. (1983). On the mechanisms of cytokinesis in animal cells. *Journal of Theoretical Biology*. https://doi.org/10.1016/0022-5193(83)90342-9

Wood, W. B. (1991). Evidence from reversal of handedness in C. elegans embryos for early cell interactions determining cell fates. *Nature*. https://doi.org/10.1038/349536a0

Table 1: Genotypes of *C. elegans* strains

Strain	**Genotype**
N2	Wild type
JCC239	*unc-61(e228)* V; *unc-119(ed3)* III; ltIs37 [pAA64; *pie-1*/mCHERRY::his-58; *unc-119 +)*] IV
JCC661	*unc-59(e1005)* I.; *unc-119(ed3)* III*; ltIs38 [pAA1; *pie-1*/GFP::PH(PLCdelta1); *unc-119 (+)*] III.; *unc-119 (+)*] III; ltIS37 [pAA64; *pie-1*/mCherry::his-58; *unc-119(+)*] IV.
MDX79	ltIs37 [pAA64; pie-1/mCHERRY::his-58; unc-119 (+)] IV; cyk-1(ges1[cyk-1::eGFP+LoxPunc-119(+)LoxP)III;unc-119(ed3)III.

* since this lesion is rescued by transgenes, its maintained presence is unknown

Figure Legends

Figure 1: Cortical rotation in *C. elegans*

(A) A schematic depiction of the use of a hand with thumb pointed towards the zygote posterior to determine the chirality of *C. elegans* cortical rotation. (B) Consecutive frames of cortical rotation (dt = 2s). Colored circles highlight cortical granules, while the corresponding colored line denotes the starting location (at t = 0s) of the granule across all time points. Scale bar = 10 microns (C) Kymograph of cortical rotation in a control cell. (D) Representative vector field outputs from OpenPIV using the same cell as in (A), before and during rotation. Arrow length represents local velocity. (E-F) Circumferential (around the anterior-posterior axis) and Posterior-directed velocities during cortical rotation over time, averaged across the length of the cell. (G-H) Averaged circumferential velocity of cortical rotation with respect to the position along anterior-posterior axis. Pale purple lines are individuals; heavy purple line is the population average (n = 6).

Figure 2: Cortical rotation is dependent on septins

(A) Rotation phenotype frequency for genetic perturbations of septins. Continuous rotation has a single period of increased velocity; intermittent rotation has several periods interspersed with periods of slower or no movement; none indicates that no rotation occurred. (B) Example kymographs of cells exhibiting intermittent or no rotation (see Figure 1 for continuous). (C-E) Circumferential velocities over time averaged across the anterior-posterior axis. Colored lines indicate individuals of the corresponding color-coded phenotype; black line is the population average (*unc-59(RNAi)* n = 12; *unc-59(e1005)* n = 9; *unc-61(e228)* n = 6); purple line is the control average (n = 6). (F-I) Quantification of mean velocity, maximum velocity, duration, and

displacement, respectively. Colored dots are individuals of the corresponding phenotype. Vertical notches are population means; horizontal lines are 95% confidence intervals. (*) $p < 0.05$; unmarked pairings are not significantly different.

Supplement to Figure 2: Anterior-to-Posterior and binned velocities of septin loss of function cells

(A-C) Posterior-directed velocities over time for *unc-59(RNAi)*, *unc-59(e1005)*, and *unc-61(e228)* cells, respectively (n = 12, n = 9, n = 6, respectively). Colored lines indicate individuals of the corresponding color-coded phenotype; black line is the population average; purple line is the control average. (D-F) Binned circumferential velocities. Populations and color denotations are the same as panels A-C. (G-I) Binned posterior-directed velocities. Populations and color denotations are the same as panels A-C.

Figure 3: Formins have a septin-dependent posterior-enrichment in the *C. elegans* zygote

(A) Schematic of intensity measurements. (B) Control and *unc-59* depleted cells exhibited CYK-1::GFP. Scale bar = 10 microns. (C) Mean intensity ratio (P/A) of CYK-1::GFP just prior to anaphase onset for control (n = 5) and *unc-59(RNAi)* (n = 4) cells. Dots are individuals; horizontal bar is population mean; vertical notches are 95% confidence interval. (*) $p < 0.01$. (D) Mean intensity ratio of CYK-1::GFP (P/A) leading up to cortical rotation. Black line is population mean (control: n = 12, UNC-59 depleted: n = 5). Gray shaded areas are 95% confidence intervals; pale green lines are linear regression for upper, middle, and lower bounds of confidence.

Supplement to Figure 3: Photobleaching adjustment for *cyk-1*::GFP cells

(A) Averaged fluorescence intensity CYK-1::GFP in cells treated with azide (n=10) (B-C) Cortical fluorescence intensities over time in CYK-1::GFP control (B, n =12) and UNC-59 depleted (C, n

= 5) cells. (D-E) Photobleaching-corrected CYK-1::GFP intensities for the same cells as in B and C. Movies were recorded on the same settings as those made to build the decay model in (A); the decay coefficient was used to calculate and add in the intensity that was lost to photobleaching.

Figure 4: Cortical rotation is dependent on the formin CYK-1

(A) Phenotype frequency for various genetic perturbations of *unc-61* and *cyk-1*. Alternating rotation changes direction at least once; continuous rotation has a single period of increased velocity; intermittent rotation has several periods interspersed with periods of slower or no movement; none indicates that no rotation occurred. (B) Example kymographs of cells exhibiting reversed handedness or alternating rotation. (C-D) Circumferential velocities over time averaged across the A-P axis. Colored lines indicate individuals of the corresponding color-coded phenotype; purple line: control average; red line: *cyk-1(RNAi)* population average (n = 10); black line: *cyk-1(RNAi)* + *unc-61(e228)* population average (n = 18); dashed line: reversed handedness. (E-H) Quantification of mean velocity, maximum velocity, duration, and displacement, respectively. Colored dots are individuals of the corresponding phenotype. Vertical notches are population means; horizontal lines are 95% confidence intervals. (*) = $p < 0.05$; unmarked pairings are not significantly different.

Supplement to Figure 4: AP and binned velocities for *CYK-1* loss of function cells

(A-B) Posterior-directed velocities over time for *cyk-1(RNAi)* and *cyk-1(RNAi)+unc-61*(e228) populations, respectively (n = 10, n = 18). Colored lines indicate individuals of the corresponding color-coded phenotype; black line is the population average; purple line is the wild-type average; red line is *cyk-1(RNAi)* average. (C-D) Binned circumferential velocities. Populations and color

denotations are the same as panels A-B. Dashed line indicates reversed handedness (E-F) Binned posterior-directed velocities. Populations and color denotations are the same as panels A-B.

Figure 5: A model for the actin cytoskeleton structure in *C. elegans* zygotes

(A) Schematic of the hypothesized structure of the actin cytoskeleton that drives rotation in adherent mammalian cells (adapted from Tee et al., 2015). Peripheral, anchored formins (blue) generate radial F-actin (orange) under torque (red) and coupled to circumferential bundles (yellow) whose contractility leads to a counter-clockwise skew (purple). (B) Summary schematics of a control *C. elegans* zygote (i) and those perturbed, exhibiting failure (ii) of, and reversed chirality (iii), cortical rotation. (C) Cut-away perspective view into the posterior pole of the *C. elegans* zygote illustrating hypothetical mechanism for cortical rotation: Membrane-anchored, posterior-enriched formins (blue) generate longitudinal (posterior-to-anterior) bundles that interact with circumferential cytokinetic ring actin bundles (yellow). Contraction in the ring could relieve chiral torque (red) within posterior-to-anterior bundles (orange), generating a right-handed rotation (purple). Septins (green) could contribute to this phenomenon by localizing/anchoring formins to the posterior focal adhesions or crosslinking within or between actin bundle populations.

Supplemental Movie 1

Time lapse of cells exhibiting (A) continuous cortical rotation (wild-type), (B) intermittent cortical rotation (*unc-59(e1005)*), (C) no cortical rotation (*unc-59(e1005)*), (D) cortical rotation with reversed handedness (*cyk-1(RNAi)*), and (E) alternating cortical rotation (*cyk-1(RNAi)*). Images were acquired at 2 second intervals. Scale bar = 10 μm.

Zaatri et al Figure 1

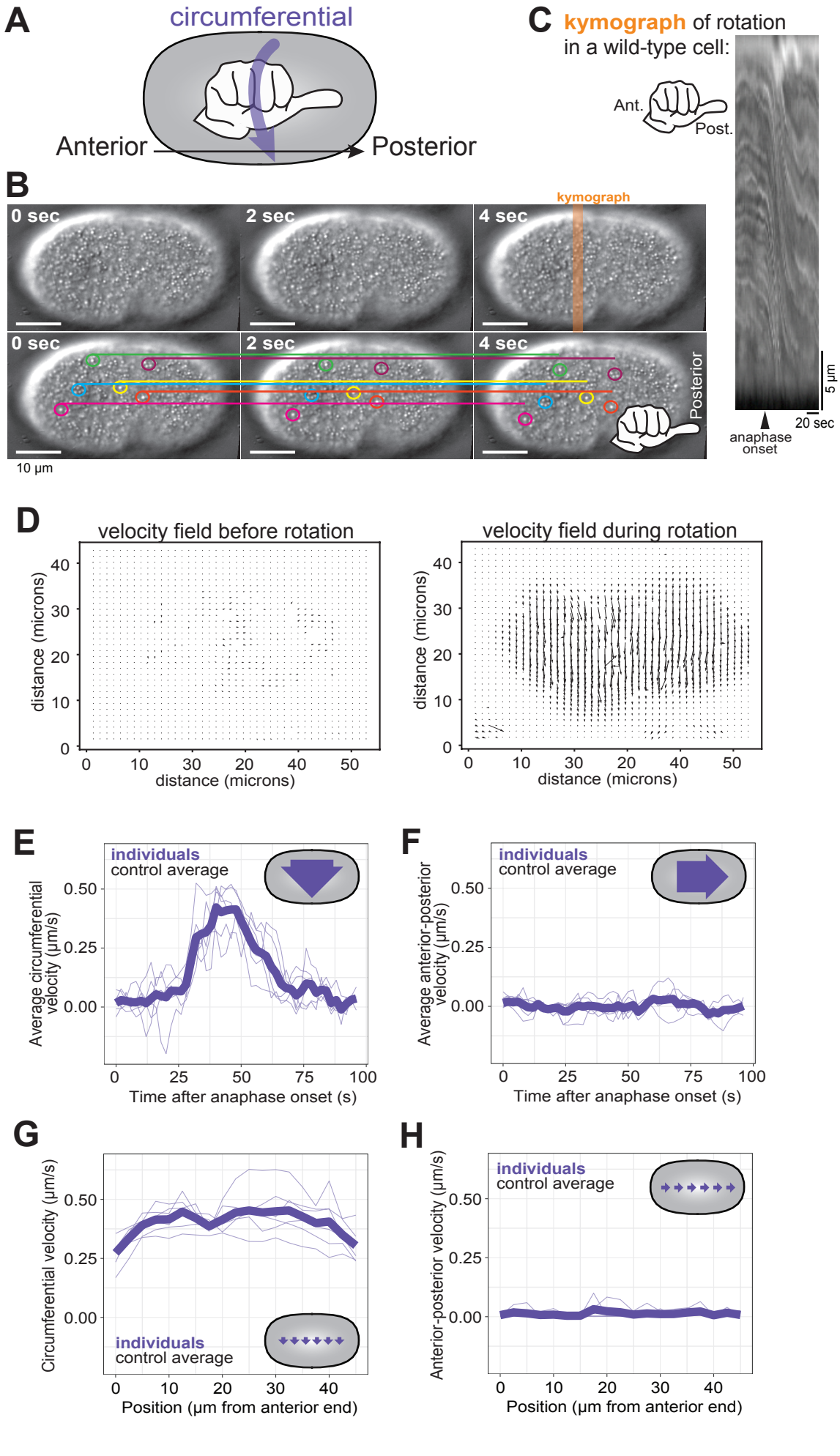

Zaatri et al Figure 2

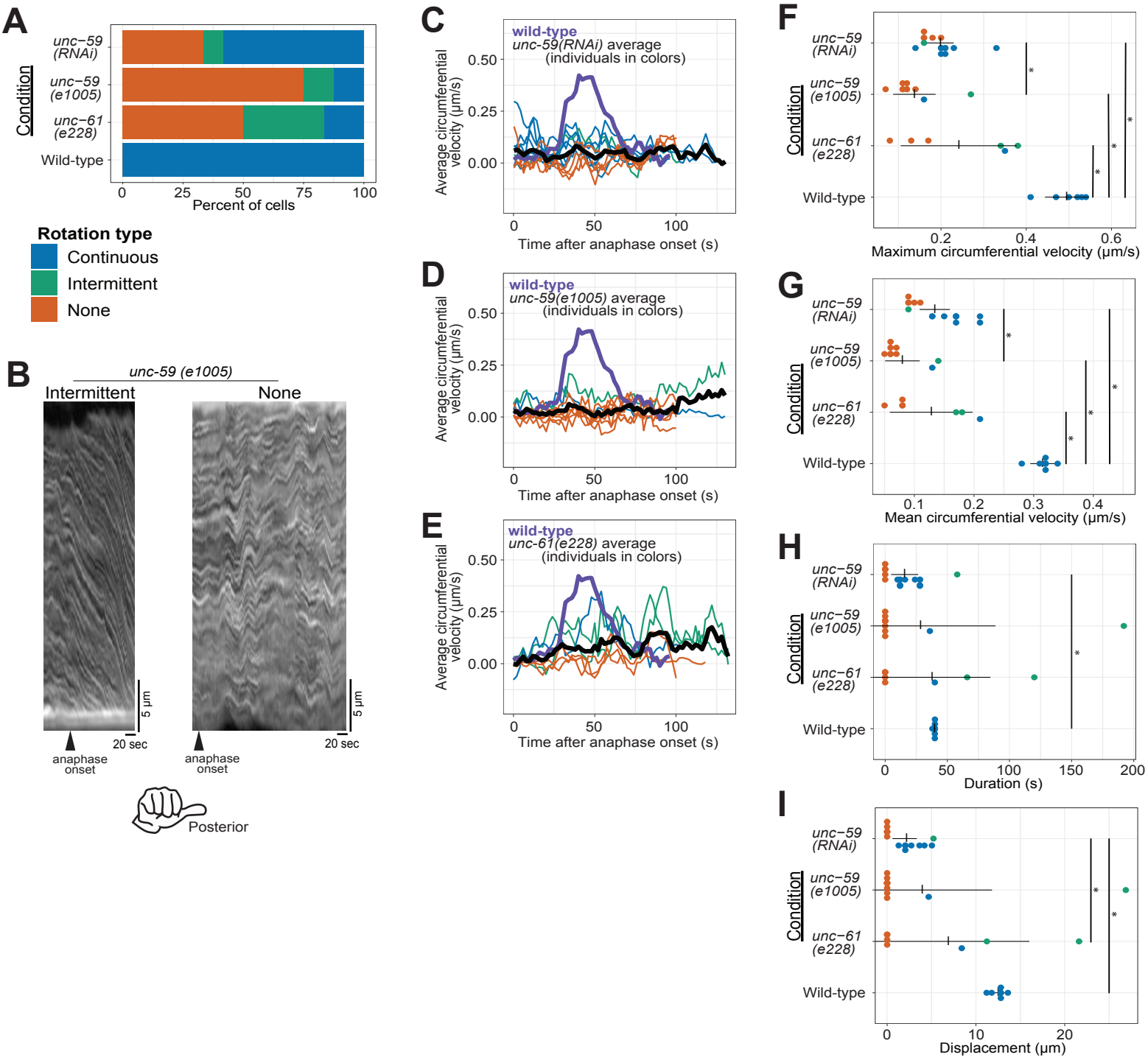

Zaatri et al Figure 2 Supplement

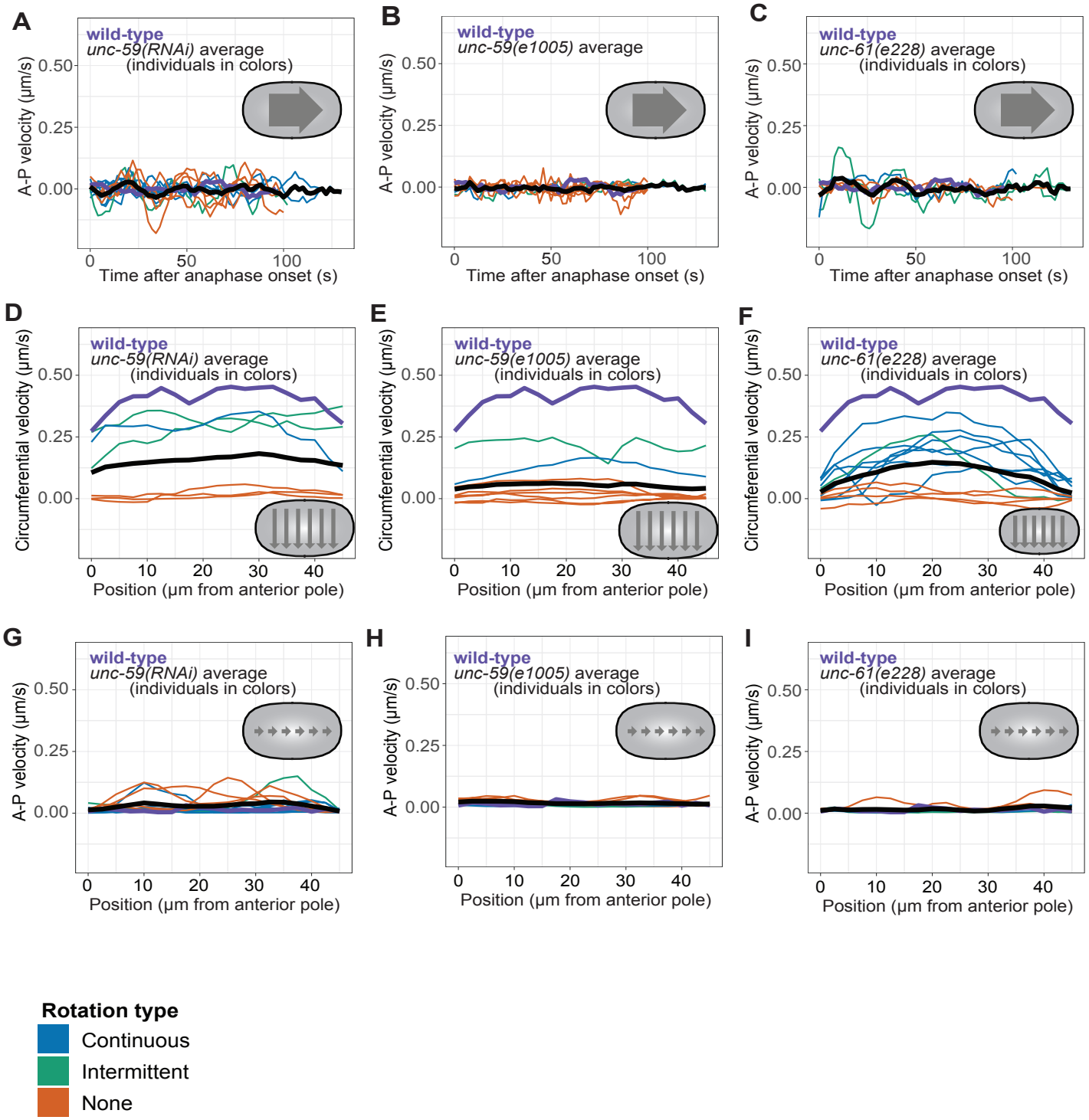

Zaatri et al Figure 3

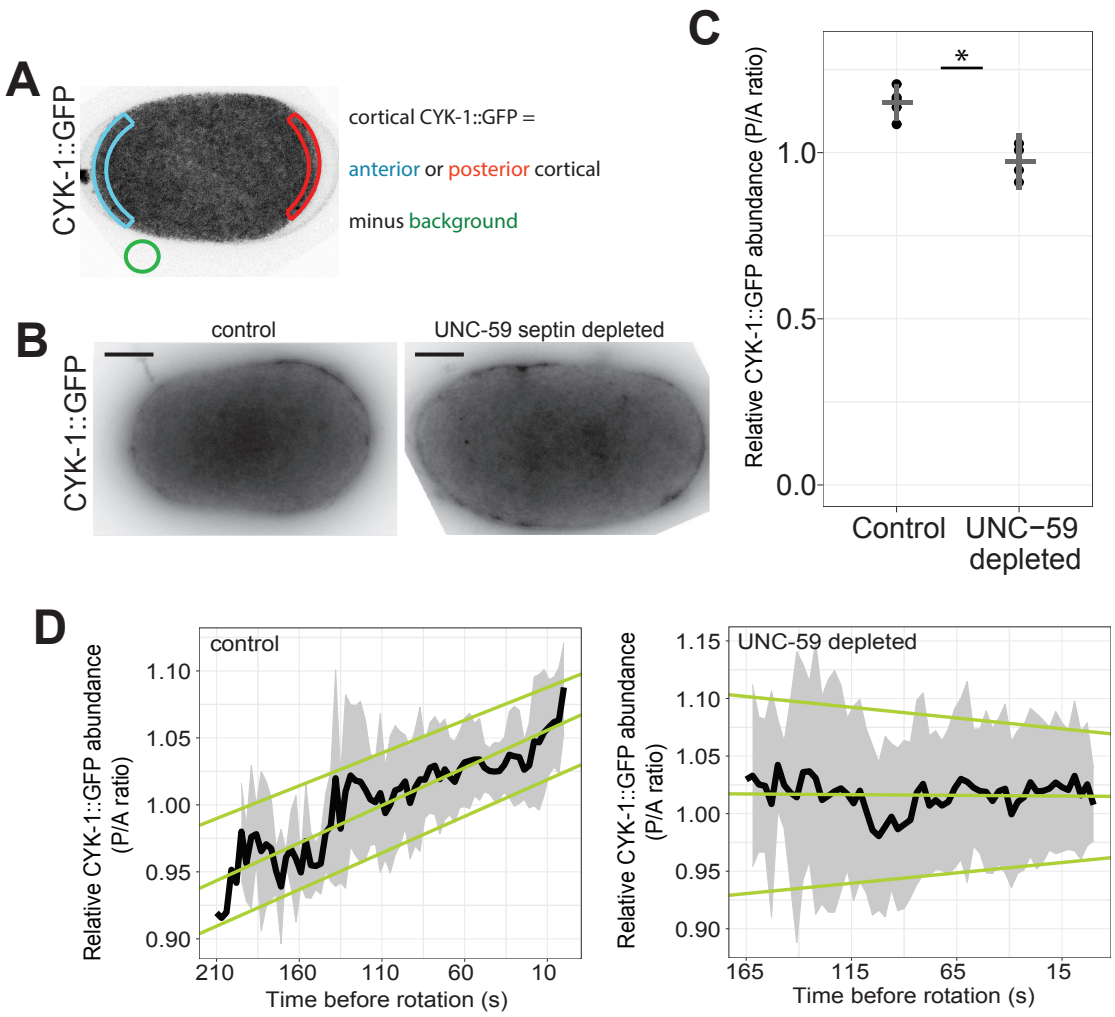

Zaatri et al Figure 3 Supplement

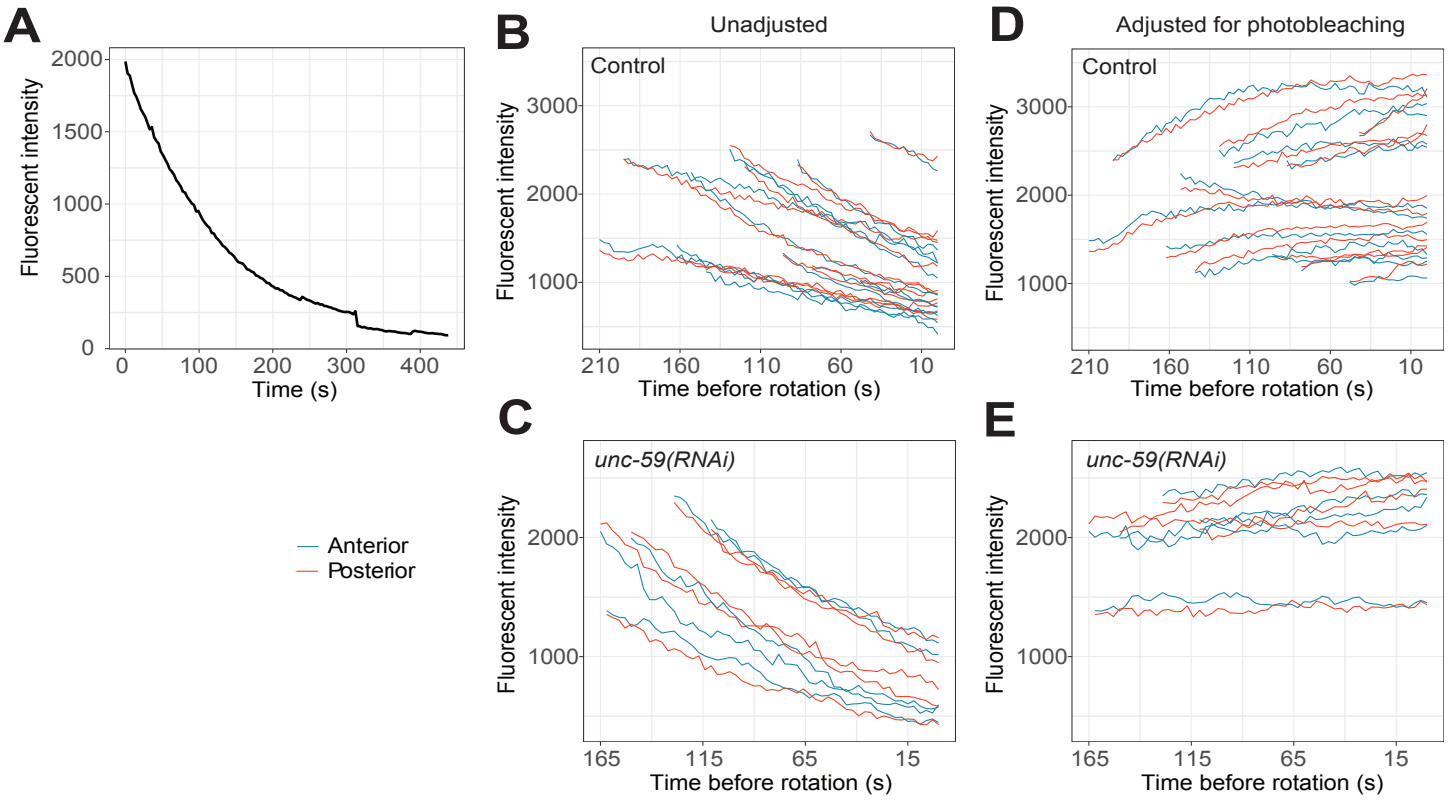

Zaatri et al Figure 4

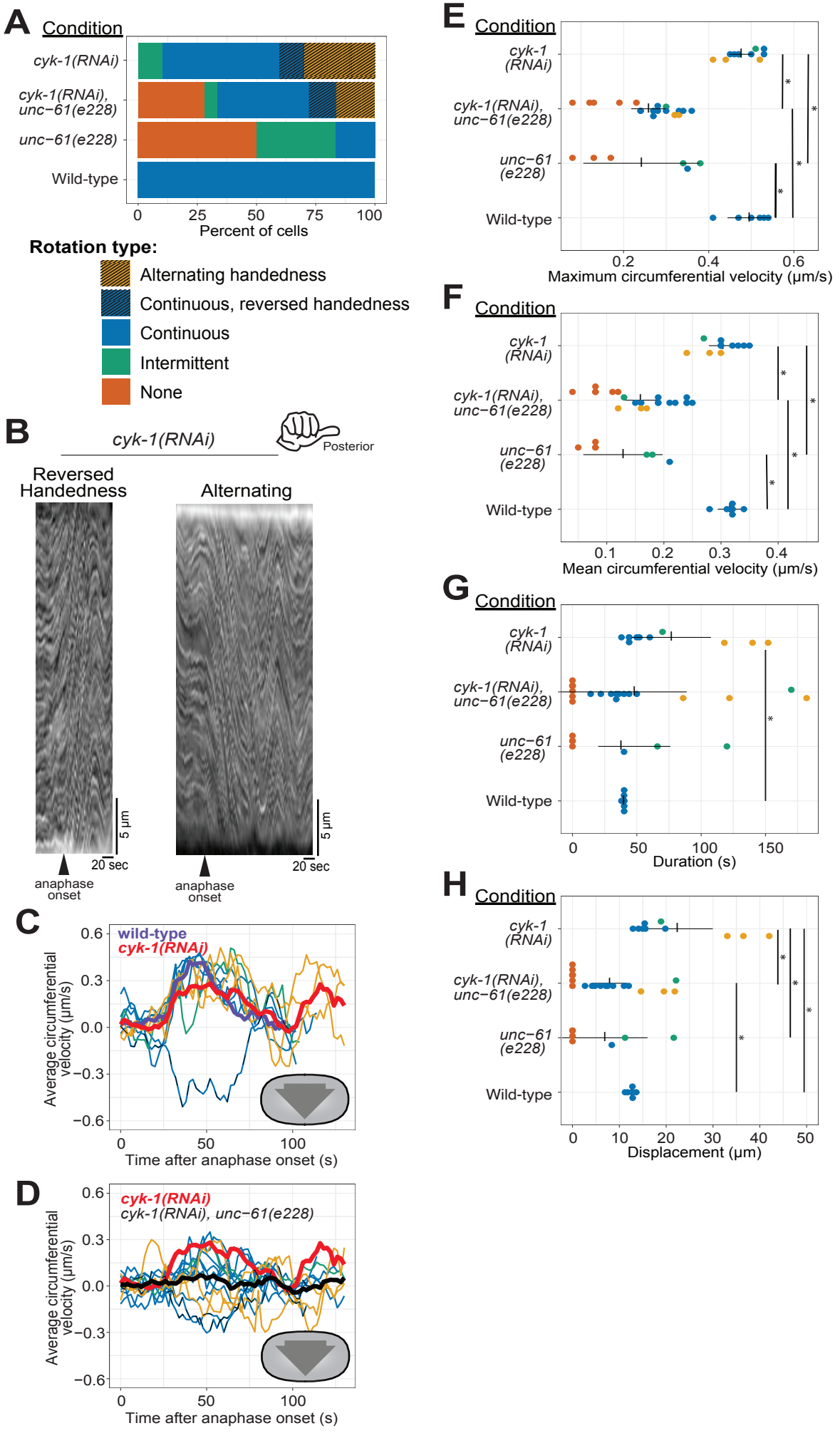

Zaatri et al Figure 4 Supplement

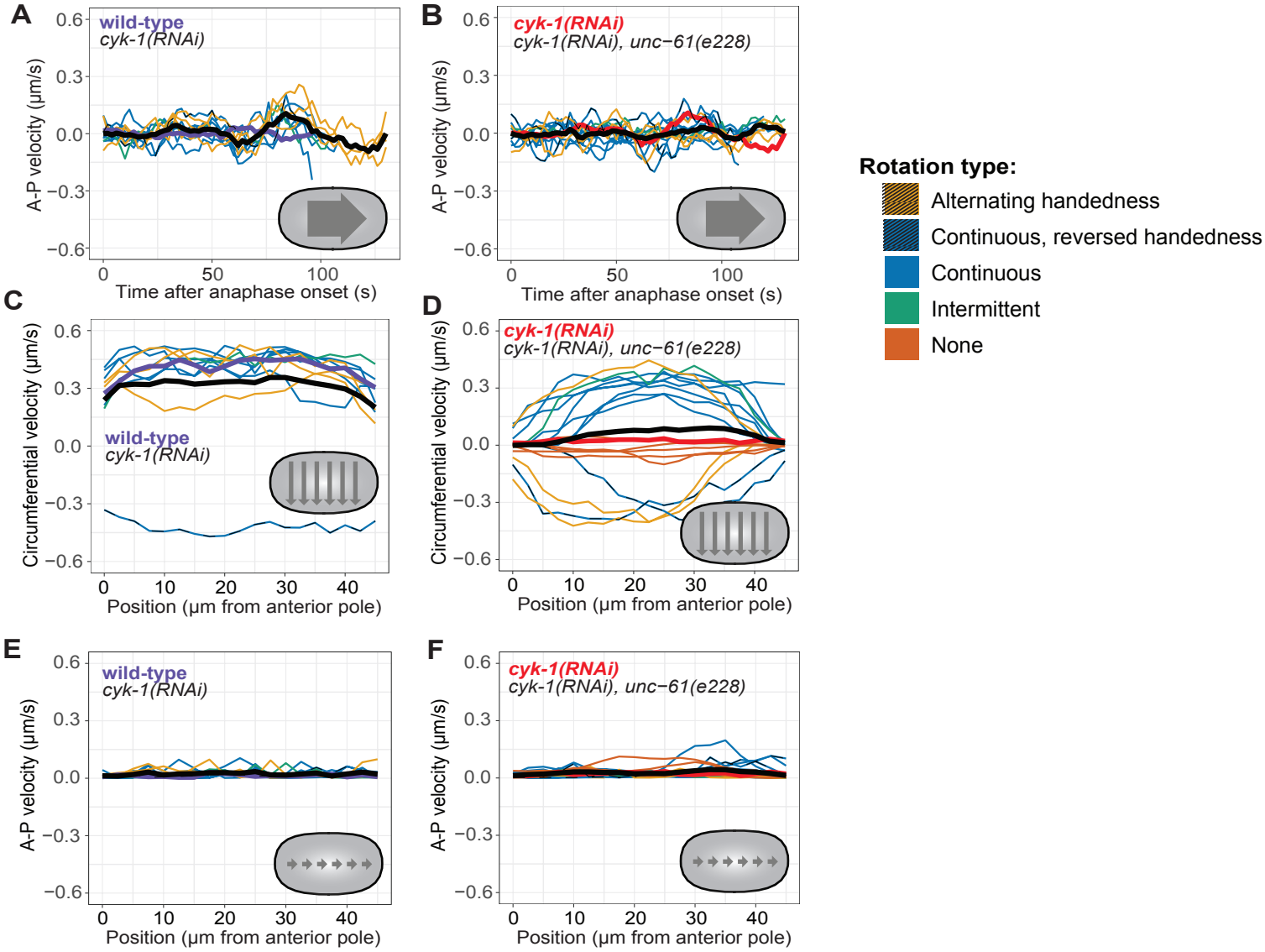

Zaatri et al Figure 5

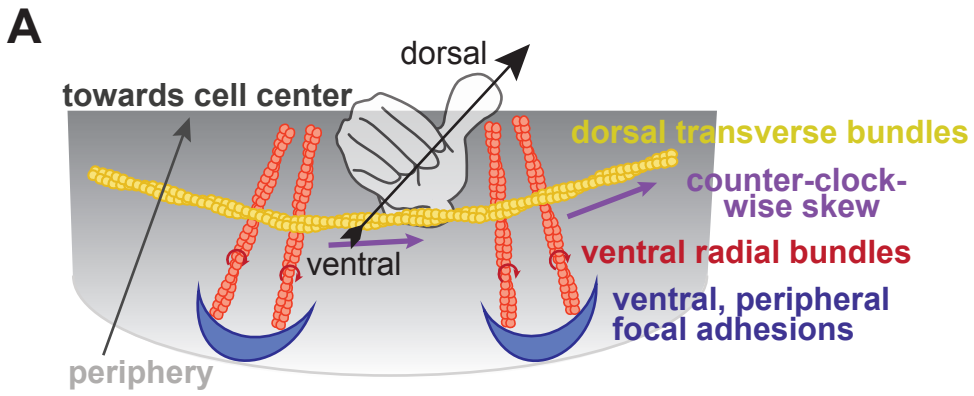

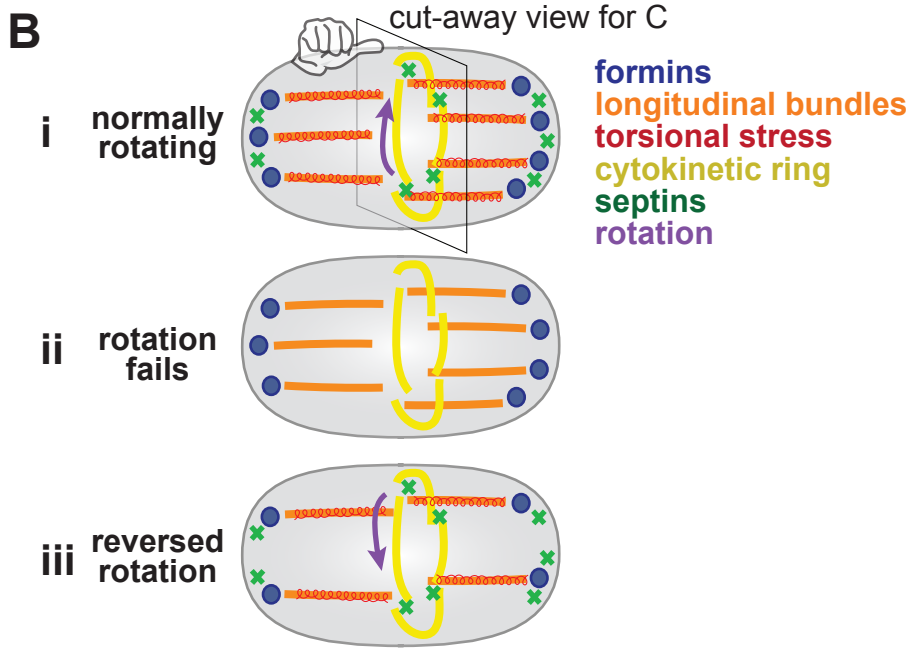

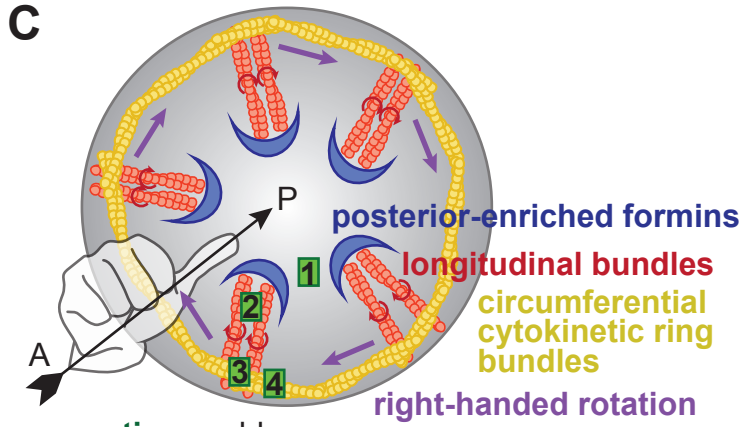

septins could:

1. anchor formins at the membrane
2. crosslink within longitudinal bundles
3. crosslink longitudinal bundles to the cytokinetic ring
4. crosslink within the cytokinetic ring